Correlation of Zero Field Splittings and Site Distortions. VII. $FeCl_4^-$ in $CsGaCl_4$ with Crystal Structure Refinement

R. Büscher and G. Lehmann
Institut für Physikalische Chemie, Westfälische Wilhelms-Universität, Münster

G. Henkel and B. Krebs
Institut für Anorganische Chemie, Westfälische Wilhelms-Universität, Münster

Z. Naturforsch. **39 a**, 1204–1207 (1984); received October 13, 1984

A crystal structure refinement for $CsGaCl_4$ resulted in considerably lower limits of error than older data from the literature. These were used for a superposition analysis of EPR data for Fe^{3+} in this compound. The experimental zero field splitting (ZFS) pattern could be very satisfactorily reproduced with the intrinsic ZFS parameter $\bar{b}_2 = 0.6\,cm^{-1}$. Thus like for other ligands $\bar{b}_2$ for Fe^{3+} is again several times larger than for the isoelectronic Mn^{2+}.

Introduction

A large body of experimental evidence has shown that for Mn^{2+} the zero field splitting (ZFS) patterns are – at least for their largest part – determined by the geometry of the first coordination shell. At the same time an increase of the intrinsic second order ZFS parameter (that is, roughly speaking, the ZFS per unit distortion) was shown to increase from small negative values for light atoms as ligands to much larger positive values for heavier atoms [1, 2]. This experimental result was also reproduced for Cl^- as ligand in quantum mechanical calculations for the superponable mechanisms based on overlap and covalency [3] showing that these contributions dominate over electrostatic ones for heavier atoms as ligand. Reported failures of the empirical superposition model (SPM) [4] can either be ascribed to effects of local relaxation around the transition metal impurities or are most likely due to electron delocalization, e.g. in the pyrite structure of MX_2 composition with X = S, Se or Te where the position of the next chalcogenide neighbor of an X_2^{2-} group is not representative for its effect on the ZFS pattern [5].

Applications of the SPM to the isoelectronic Fe^{3+} are much more scarce and so far were restricted to O^{2-} [6–9], F^- [10, 11] and S^{2-} [12].

We here report EPR data for Fe^{3+} in single crystal $CsGaCl_4$ together with a crystal structure refinement for the host compound which confirm validity of the SPM in this case and allowed determination of the intrinsic ZFS parameter $\bar{b}_2$ for $FeCl_4^-$ for the first time.

Reprint requests to Prof. Dr. G. Lehmann, Institut für Physikalische Chemie, Universität Münster, Schloßplatz 4, D-4400 Münster.

Experimental

Single crystals of $CsGaCl_4$ were grown by slow evaporation of acidified aqueous solutions, but with 1 mole % of $GaCl_3$ replaced by $FeCl_3$. The yellow crystals grew with by far largest elongation along the *b*-axis. They were oriented using the X-ray precession method with only a thin edge of the crystal exposed to the X-ray beam. The Q-band EPR spectrometer used has been previously described in detail [13] just as the computer programs for calculation of the fine structure parameters. The sign of b_2^0 was determined at X-band from the relative intensity changes of low and high field transitions [14] between 300 and about 20 K where the lower temperature was obtained using a Displex Cryogenic helium refrigeration system model CSA-202G of Air Products and Chemicals Inc.

Results and Discussion

X-ray data collection and structure refinement

A single crystal of $CsGaCl_4$ was sealed in a glass capillary and used for X-ray measurements. X-ray intensity data were collected on a Syntex $P2_1$ four-circle diffractometer equipped with a molybdenum tube, a graphite monochromator and a scintillation

0340-4811 / 84 / 1200-1204 $ 01.30/0. – Please order a reprint rather than making your own copy.

counter. During data collection the crystal was cooled by a cold stream of gaseous nitrogen. The unit cell parameters were calculated from a least-squares fit of the angular settings of 15 carefully centred high-order reflexions. They are given in Table 1 together with relevant information concerning details of data collection and structure refinement. The periodically recorded intensity of a standard reflexion (230) indicated stable conditions during data collection. The intensity data were corrected for anisotropic absorption effects using intensity profiles of selected reflexions (ψ-scan method) and reduced to structure amplitudes by Lorentz and polarization corrections. The structure of $CsGaCl_4$, which is isomorphous with $BaSO_4$, has initially been described by Gearhart, Beck and Wood in 1975 [15]. Starting from the parameters reported therein, the refinement of the coordinates and anisotropic thermal vibrations of all atoms together with an anisotropic extinction coefficient and a common scale factor by full-matrix least-squares methods resulted in highly improved positional and thermal parameters. In the refinement procedures atomic scattering factors for spherical neutral atoms were used taking anomalous scattering into account [16]. The atomic coordinates and thermal parameters of the final structural model are summarized in Table 2. The bond distances and valence angles within the slightly distorted $GaCl_4$ tetrahedron are given together with the closest Cs ... Cl contacts in Table 3.

Table 1. $CsGaCl_4$: Crystal data, experimental conditions and details of structure refinement.

Formula	$CsGaCl_4$
Formula weight	344.43
Crystal dimensions	ca. $0.3 \times 0.2 \times 0.15$ mm
Temperature	$-115\,^{\circ}C$
Crystal system	orthorhombic
Space group	Pnma
a	11.610(3) Å
b	7.064(2) Å
c	9.339(3) Å
V	765.8 Å^3
Z	4
Calculated density	2.987 gcm^{-3}
Absorption coefficient	98.0 cm^{-1}
Radiation	MoK_α ($\lambda = 0.71069$ Å)
Data collection range	$4^\circ < 2\theta < 54^\circ$
Scan speed	variable (between 5 and 30° min^{-1}, depending on intensity)
Scan mode	$\theta - 2\theta$ – scan
No. of independent data collected	902
No. of data used ($\lvert F_0\rvert > 3.92\,(F_0)$)	864
No. of variables	35
$R_1 = \Sigma \lvert F_0\rvert - \lvert F_c\rvert / \Sigma \lvert F_0\rvert$	0.0316
$R_2 = [\Sigma w(\lvert F_0\rvert - \lvert F_c\rvert)^2 / \Sigma w \lvert F_0\rvert^2]^{1/2}$ ($w = [(\sigma^2(F_0)) + 0.01 \times F_0^2]^{-1}$)	0.0440

EPR

For arbitrary orientations of the magnetic field two magnetically non-equivalent EPR spectra of Fe^{3+} are observed. They coincide for the magnetic field perpendicular to either a- or c-axis. The magnetic y-axis coincides with the crystal b-axis. In Fig. 1 part of a slightly split Q-band spectrum is shown. The signals are rather broad ($H_{pp} \gtrsim 5$ mT), most likely due to unresolved hyperfine splitting from the ^{35}Cl and ^{37}Cl nuclei. A rotational diagram also showing the forbidden ($\Delta M_s > 1$) transitions at lower magnetic fields is presented in Figure 2. From this and additional measurements for $B_0 // b$ the following parameters were obtained:

$$b_2^0 = 0.1081\ (1)\ \text{cm}^{-1};\quad b_2^2 = 0.0795\ (1)\ \text{cm}^{-1}.$$

The magnetic z-axis was found to lie in the $a-c$ plane 10.1° from the a-axis. The fourth order fine structure parameters were zero within the limits of error. Although experimental as well as theoretical evidence favor a positive sign of b_2^0, it could not be determined with absolute certainty. While some transitions clearly indicated a positive sign, a few

Table 2. $CsGaCl_4$: Atom coordinates and coefficients of the anisotropic temperature factors.

	x	y	z	B_{11}	B_{22}	B_{33}	B_{12}	B_{13}	B_{23}
Cs	0.18019(3)	0.25	0.16611(4)	1.38(2)	2.91(2)	2.33(2)	0.0	−0.28(1)	0.0
Ga	0.07129(5)	0.25	0.69293(7)	1.74(3)	1.65(3)	1.43(3)	0.0	−0.21(2)	0.0
Cl(1)	−0.0936(2)	0.25	0.5863(3)	4.2(1)	6.8(2)	6.7(2)	0.0	−4.0(1)	0.0
Cl(2)	0.2164(2)	0.25	0.5492(2)	5.13(9)	3.03(8)	2.70(7)	0.0	2.39(7)	0.0
Cl(3)	0.0841(1)	0.0026(2)	0.8305(1)	2.39(5)	1.72(4)	2.42(5)	−0.02(3)	0.48(3)	0.44(3)

Table 3. $CsGaCl_4$: Selected distances and angles.

Ga Coordination	
Distances [Å]	
Ga–Cl(1)	2.158(3)
Ga–Cl(2)	2.154(3)
Ga–Cl(3)	2.174(1)
Ga–Cl(3)^{I}	2.174(1)
Angles [°]	
Cl(1)–Ga–Cl(2)	114.0(1)
Cl(1)–Ga–Cl(3)	109.5(1)
Cl(1)–Ga–Cl(3)^{I}	109.5(1)
Cl(2)–Ga–Cl(3)	108.4(1)
Cl(2)–Ga–Cl(3)^{I}	108.4(1)
Cl(3)–Ga–Cl(3)^{I}	107.0(1)
Cs Coordination	
Distances [Å]	
Cs ... Cl(1)^{II}	3.529
Cs ... Cl(2)	3.602
Cs ... Cl(2)^{III}	3.887
Cs ... Cl(2)^{IV}	3.887
Cs ... Cl(3)^{V}	3.758
Cs ... Cl(3)^{VI}	3.758
Cs ... Cl(3)^{IV}	3.610
Cs ... Cl(3)^{VII}	3.610
Cs ... Cl(3)^{VIII}	3.549
Cs ... Cl(3)^{IX}	3.549

Symmetry code:
I: x, 0.5-y, z; II: $0.5+x$, $0.5-y$, $0.5-z$; III: $0.5-x$, $-0.5+y$, $-0.5+z$; IV: $0.5-x$, $0.5+y$, $-0.5+z$; V: x, y, $-1+z$; VI: x, $0.5-y$, $-1+z$; VII: $0.5-x$, $-y$, $-0.5+z$; VIII: $-x$, $-y$, $1-z$; IX: $-x$, $0.5+y$, $1-z$

signals with larger change in halfwidths between 300 and 20 K gave the opposite result. Measurements at liquid helium temperature could perhaps resolve this ambiguity.

Superposition analysis

The observed splitting pattern is consistent with substitution of Ga on the $a-c$ mirror plane by Fe. Thus the observed ZFS pattern can be directly compared with that calculated from the distortion of the $GaCl_4$ tetrahedron. $R_0 = 219$ pm from $CsFeCl_4$ [17] and $t_2 = 7$ were used for calculation of the distortion diagrams in Figure 3. With $\overline{b_2} = 0.60\ (11)\ cm^{-1}$ the splitting diagram calculated from the EPR data closely matches the distortion diagram calculated from our crystal structure data. Within the limits of error of $\pm 6°$ for the distortion diagram the positions of the z- and x-axes resp. also almost coincide. The older crystal structure data [15] clearly have too large limits of error to allow a meaningful test.

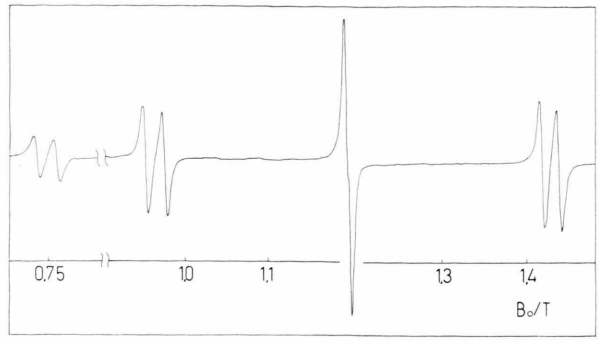

Fig. 1. Part of the EPR spectrum of $CsGaCl_4$:Fe at 33.956 GHz and room temperature for the magnetic field perpendicular to b and 10° from a.

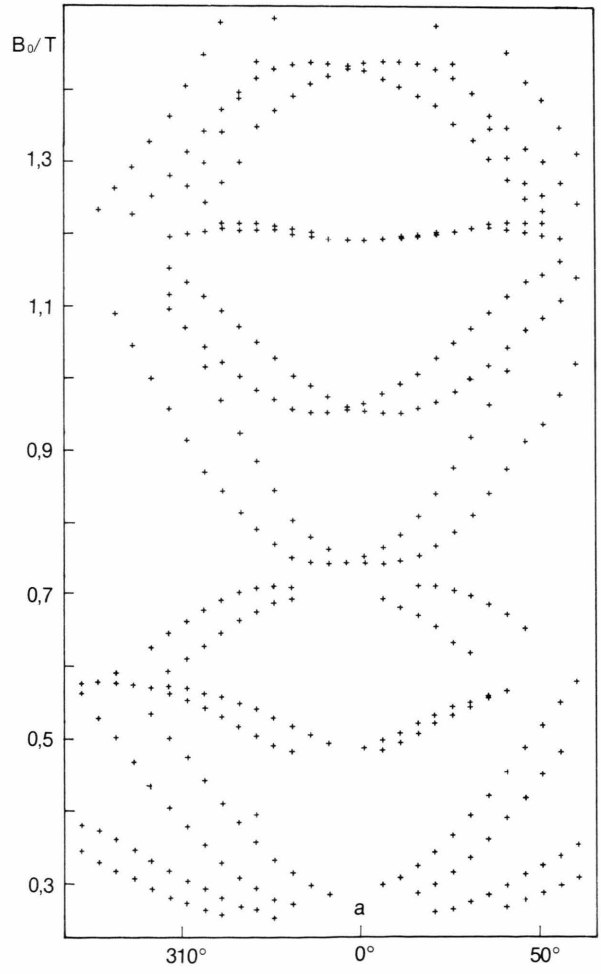

Fig. 2. Angular variation of the EPR spectrum of $CsGaCl_4$: Fe at 33.956 GHz for rotation around the b-axis. The $\Delta M_S > 1$ transitions at low fields are not shown in Figure 1.

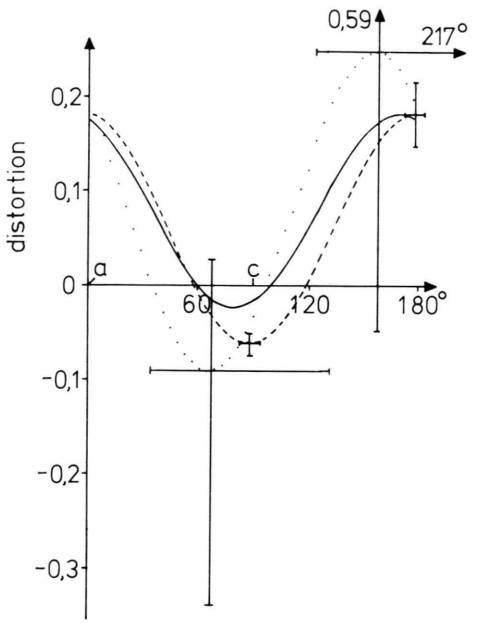

◀ Fig. 3. Comparison of measured (full curve, "splitting diagram") and calculated zero field splitting patterns for Fe^{3+} in $CsGaCl_4$ (dashed and dotted curves from crystal structure data of this work and Ref. [15] resp.) in the $a-c$ mirror plane. The full curve is given by

$$\frac{1}{0.6}[(3\cos^2\vartheta - 1)\, b_2^0 + \sin^2\vartheta \cdot b_2^2]$$

where ϑ is the angle between B_0 and the magnetic z-axis. The distortion diagrams (dashed and dotted curves) are given by

$$\sum_{i=1}^{4} (3\cos^2\Theta - 1)\left(\frac{219}{R_i}\right)^7,$$

where Θ_i are the angles of the $Ga-Cl_i$ bonds with the particular direction.

Thus also in this case the SPM works remarkably well. Like in the cases of F^-, O^{2-} and S^{2-} the intrinsic ZFS parameter for Cl^- is several times larger for Fe^{3+} than it is for Mn^{2+}. Calculations of the superponable overlap and covalency contributions for $FeCl_4^-$ would be desirable, but are not yet feasible due to lack of suitable experimental data for the overlap and covalency parameters. Investigations of $CsGaBr_4$:Fe are underway in our laboratories to extend these investigations to still heavier ligands.

Acknowledgement

This work was supported by grants from the Deutsche Forschungsgemeinschaft.

[1] M. Heming and G. Lehmann, Chem. Phys. Letters **80,** 235 (1981).
[2] M. Heming, Dissertation, Münster 1983.
[3] M. Heming, S. Remme, and G. Lehmann, Ber. Bunsenges. physik. Chem. **88,** 946 (1984).
[4] D. J. Neumann and W. Urban, Adv. Phys. **24,** 793 (1975).
[5] S. Remme and G. Lehmann, to be published.
[6] D. J. Newman and E. Siegel, J. Phys. **C9,** 4285 (1976).
[7] E. Siegel and K. A. Müller, Phys. Rev. **B20,** 3587 (1979).
[8] G. Lehmann, Phys. stat. sol. (b) **99,** 623 (1980).
[9] P. Novák and L. Vosika, Czech. J. Phys. **B 33,** 1134 (1983).
[10] H. S. Murrieta, J. O. Rubio, and G. S. Aguilar, Phys. Rev. **B19,** 5516 (1979); H. S. Murrieta, F. J. Lopez, J. O. Rubio, and G. S. Aguilar, J. Phys. Soc. Jpn. **49,** 499 (1980).
[11] A. Leblé, J. J. Rousseau, J. C. Fayet, and C. Jacoboni, Sol. State Commun. **43,** 773 (1982).
[12] B. Frick and D. Siebert, Z. Naturforsch. **37a,** 1005 (1982).
[13] H. Sachs and G. Lehmann, Phys. stat. sol. (b) **92,** 417 (1979).
[14] A. Abragam and B. Bleaney, Electron Paramagnetic Resonance of Transition Ions, Oxford 1970, p. 160 ff.
[15] R. C. Gearhart, Jr., J. D. Beck, and R. H. Wood, Inorg. Chem. **14,** 2413 (1975).
[16] International Tables for X-ray Crystallography, Vol. IV, Kynoch Press, Birmingham 1974, p. 99 ff.
[17] G. Meyer, Z. anorg. allg. Chem. **436,** 87 (1977).